

Imaging an off-plane shear wave source with two-dimensional phononic-crystal lens

Chen-Yu Chiang and Pi-Gang Luan

*Wave Engineering Laboratory, Department of Optics and Photonics,
National Central University, Jhungli 320, Taiwan*

Abstract

A two dimensional flat phononic crystal (PC) lens for focusing off-plane shear waves is proposed. The lens consists of a triangular lattice hole-array, embedded in solid matrix. Self-collimation effect is employed to guide the shear waves propagating through the lens along specific directions. Dirichlet-to-Neumann Maps (DtN) method is employed to calculate the band structure of the PC, which can avoid the problems of bad convergence and fake bands automatically in the void-solid PC structure. When the lens is illuminated by the off-plane shear waves emanating from a point source, a subwavelength image appears in the far-field zone. The imaging characteristics are investigated by calculating the displacement fields explicitly using the multiple-scattering method, and the results are in good agreement with the ray-trace predictions. Our results may provide insights for designing new phononic devices.

PACS numbers: 41.20.Jb, 43.20.El

Phononic crystals (PC) are artificial periodic elastic media made for controlling the propagation of acoustic/elastic waves. The propagating modes of the elastic waves in PC are Bloch waves, and their dispersion relations form the phononic band structures, containing passbands and bandgaps. Various structures for reflecting, trapping, and guiding acoustic/elastic waves relying on the existence of PC bandgaps have been proposed and studied [1–9]. Besides the bandgaps, the phononic passbands are also useful and have interesting properties. When operating in the linear region well below the top of the first band (i.e., the long-wavelength region), a PC behaves just like a homogeneous medium, and lens-like devices can be constructed from it [10, 11]. Recently, the study of wave propagation behaviors beyond the long-wavelength region has attracted a great deal of interest. It has been shown that a slab of PC operating at an appropriate frequency can focus the acoustic waves emanating from a point source to form a subwavelength image, overcoming the diffraction limit [12, 13].

To achieve the slab imaging ability, either negative refraction or anomalous refraction is required [14–17], which means the direction of the averaged Pointing vector $\langle \mathbf{S} \rangle$ must have a component antiparallel to the Bloch wavevector \mathbf{k} or some effective Bloch wavevector $\mathbf{k}_{ef} = \mathbf{k} - \mathbf{k}_0$, i.e., $\mathbf{k}_{ef} \cdot \langle \mathbf{S} \rangle < 0$. Here \mathbf{k}_0 stands for certain symmetry point in the first Brillouin zone or on the zone boundary, such as the M point for the square-lattice structure of PC. Recently, it has been pointed out that the PC band structure can also provide other wave guiding mechanisms such as self-collimation [18–21] and canalization [17, 22]. Using these mechanisms, waves can be guided along certain specific directions inside the slab and thus some desired devices such as hyperlens can be realized [23].

Up to now most of the studies on the negative refraction or subwavelength imaging phenomena adopted the PC that sustain pressure waves, and the discussions on similar phenomena in solid elastic media are relatively few [15–17]. In this letter, we employ the self-collimation effect of PC to design a flat lens for focusing off-plane pure shear wave. The lens consists of a triangular lattice hole-array embedded in a solid matrix. When the lens is illuminated by the off-plane shear waves emanating from a point source, a subwavelength image appears in the far-field zone. The imaging characteristics for a finite lens are investigated by calculating the displacement fields using the *Multiple Scattering* (MS) method [11, 24]. The PC band structure is obtained with the *Dirichlet-to-Neumann Maps* (DtN) method [25, 26]. Effective negative refractive index of the PC can be extracted from the

equal frequency contour (EFC), and the image points can be predicted according to Snell's law. The results are in good agreement with the calculations of field distributions.

It is known that in calculating the band structure of the fluid-solid or void-solid PC, the traditional plane wave expansion (PWE) method encounters the problems of bad convergence and fake flat bands [27, 28]. These problems can be resolved by replacing the void part with a "pseudosolid" or "low impedance material" [29, 30], which is an imagined solid material having a very low density and appropriately chosen wave speed (usually very large). When these material parameters are properly chosen, the flat band will appear only in the uninterested high frequency range, and thus we can safely obtain the desired band structure in the moderate frequency range. Although this modified PWE method can indeed avoid the flat band problem, there is no definite way of choosing the material parameters of the pseudosolid, and usually some experiences are needed. In order to reduce the uncertainty, we adopt instead the DtN method to calculate the band structure of the PC. Since this method can be applied to the void-solid case directly, the flat band problem disappears automatically. Up to now DtN method has only been used in calculating the band structures or guided modes of two-dimensional photonic crystal (PhC) systems, however, there is no essential difference mathematically between the two-dimensional (2D) electromagnetic (EM) and acoustic (AC) systems if the polarizations of the waves are properly chosen. For example, the transverse-magnetic (TM) wave propagating in a 2D PhC and the pure shear wave propagating in a 2D solid PC are governed by the same kind of scalar wave equation. Thus an EM wave problem can be easily translated to an AC wave problem and a one-to-one correspondence can be established between these two systems [31]. This consideration implies that DtN method can be used in the present case of pure shear wave. A detailed description of DtN method will be given later.

Since in our chosen structure the off-plane shear wave cannot penetrate into the holes, the band structure of the PC is determined only by the geometrical factors (the hole size, lattice constant, and lattice type) and the material parameters (the mass density and the Lamé constant for shear wave) of the host medium. In fact, if the lattice type, hole shape and the filling fraction of the hole in a unit cell are all given, the band structure of the PC becomes universal [33, 34] if the dimensionless frequency $\omega a/2\pi c_t$ is used as the frequency variable. Here c_t represents the propagation speed of the shear wave in the host medium and a is the lattice constant. If we replace the original host medium by another material,

the universal band structure predicts that identical wave phenomena can happen in this new PC, usually in a different frequency or for a different PC size. Note that although for non-dispersive host media the band structure for a PC consisting of several materials can also be expressed in a size-independent universal manner, the material-independence is a unique property of the hole-array PC. Moreover, in this case the (shear) wave speed is the only relevant material parameter to determine the band structure.

To be more specific, we choose aluminum as the host medium ($\rho = 2.692\text{g/cm}^3$, $c_t = 3220\text{m/s}$). The lattice type is triangular, the lattice constant is a , and the radius of the holes is $r_0 = 0.4a$. An off-plane monochromatic shear wave $\mathbf{u}(\mathbf{r}, t) = \hat{\mathbf{z}}u(\mathbf{r})e^{-i\omega t}$ propagating (in plane) in the host medium satisfies the Helmholtz equation

$$\nabla^2 u(\mathbf{r}) + k_t^2 u(\mathbf{r}) = 0. \quad (1)$$

Here $u(\mathbf{r}) = u(x, y)$ represents the amplitude of the displacement, $k_t = \omega/c_t$ is the wave number of the shear wave, and the $\nabla^2 = \partial^2/\partial x^2 + \partial^2/\partial y^2$ is the 2D Laplacian operator because u does not depend on z . Since the holes are all circular, displacement field in the host medium around a hole (say, the i th hole) can be expressed as a sum of cylindrical waves:

$$u(\mathbf{r}) = \sum_{n=-\infty}^{\infty} C_n \left(J_n(k_t r) - \frac{J'_n(k_t r_0)}{Y'_n(k_t r_0)} Y_n(k_t r) \right) e^{in\phi}. \quad (2)$$

Here $r = |\mathbf{r} - \mathbf{r}_i|$ is the magnitude of the position vector relative to the center of the i th hole, and $\phi = \phi_{\mathbf{r}-\mathbf{r}_i}$ is its azimuthal angle. To derive this expression, the boundary condition that the shear stress vanishes along the hole boundary has been applied.

Equation (2) says that both u and its first derivative along any direction are determined by the coefficients C_n . Therefore, a DtN map between u and its normal derivative $\partial u/\partial n$ along the boundary of a unit cell can be established. Using this relation together with Bloch boundary conditions $u(\mathbf{r} + \mathbf{a}_1) = e^{i\mathbf{k}\cdot\mathbf{a}_1} u(\mathbf{r})$, $u(\mathbf{r} + \mathbf{a}_2) = e^{i\mathbf{k}\cdot\mathbf{a}_2} u(\mathbf{r})$, the Bloch wave modes $u(\mathbf{r})$ and the PC band structure can be determined [25, 26]. Here $\mathbf{a}_{1,2}$ represent the primitive lattice vectors, and \mathbf{k} is the Bloch wave vector. Equation similar to (2) but expanded as sum of Bessel and Hankel functions can also be derived. Using that equation, together with the fact that the incident wave around a hole comes from the scattered waves of other holes and the waves from the sources, a matrix equation relating the scattering coefficients and the source coefficients can be established. Solving this matrix equation then gives us the displacement field in the host medium under the illumination of the sources [11, 24].

The band structure and the EFC of the PC calculated using DtN method are shown in Fig.1 (a) and 1(b). We have also calculated the same band structure using the pseudosolid method, and no visible difference between the results of these two methods can be found. The accuracy of the band structure is thus confirmed. The two inclined straight lines in Fig. 1(a) stand for the “sound lines” of the host medium. To focus the shear waves emanating from a point source, we choose $k_t a / 2\pi = \omega a / 2\pi c_t = 0.6$ as the operating (reduced) frequency. The EFC of the PC at this frequency looks like a hexagon, which occupies an area a little smaller than the corresponding circular EFC of the host medium. The frequency surface $\omega(\mathbf{k})$ of the PC in the 2nd band around the Γ point has a negative curvature (negative effective phonon mass), which leads to $\mathbf{k} \cdot \mathbf{v}_g < 0$, and thus negative refraction can occur. Here $\mathbf{v}_g = \nabla_{\mathbf{k}}\omega$ is the group velocity, pointing in the direction of the greatest rate of increase of ω and is perpendicular to EFC. It can also be shown that the direction of \mathbf{v}_g is the same as the direction of energy flow (averaged Poynting vector) [32]. When a plane wave of wave vector \mathbf{k} is incident upon a PC, the refracted wave vector \mathbf{k}' can be determined by three rules. First, the incident and refracted waves have the same frequency. Thus the tips of \mathbf{k} and \mathbf{k}' are located on the host and PC EFCs, respectively. Second, the wave phase on the two sides of the host-PC interface must be the same, which means the tangential component of \mathbf{k} is equal to that of \mathbf{k}' . Third, the normal component of \mathbf{v}_g does not change sign in the refraction process, which is a consequence of the energy conservation law $\nabla \cdot \langle \mathbf{S} \rangle = 0$ for monochromatic wave. An illustration of this refraction process in terms of the \mathbf{k} -space description and its corresponding \mathbf{r} -space configuration is shown in Fig.1(b). The thick black arrows represent the incident and refracted wave vectors, whereas the pink arrows indicate the \mathbf{v}_g (energy flow) directions. Hereafter we always assume ΓK be the orientation of the host-PC interface. The EFC plot in Fig. 1(b) also indicates that if the incidence angle is in the interval $(-\pi/3, \pi/3)$, wave can penetrate into the PC and the refraction angle of ray (energy flow) are almost fixed at $\pm\pi/6$. This is caused by the self-collimation effect of the hexagonal shaped EFC. On the other hand, if the incident angle is beyond $(-\pi/3, \pi/3)$, no refracted wave can be excited, and the incident wave will be totally reflected. These phenomena are illustrated in Fig.2 (a)-(c). Here we use Gaussian beams as incidence waves instead of plane waves. The Gaussian source used in these simulations is formed by giving a Gaussian strength profile along 20 aligned point sources distributed evenly within $4a$. The incidence angles in Fig. 2(a), (b) and (c) are $\pi/18$ (10°) and $2\pi/9$ (40°), and $\pi/3$ (60°),

respectively. The $\pi/6$ bending refraction beams in the first two cases and the almost totally reflected beam in the third case are clearly observed.

The self-collimation effects in square lattice PC or PhC have already been discussed by some researchers [17–21], however, to our knowledge, this effect in triangular lattice structures has not yet been utilized as a means to design an acoustic lens for focusing sound. Here we show its applicability. Unlike most previously designed flat lens using circular EFC, we use a hexagonal EFC to achieve this goal. Usually a size-matched circular EFC having an effective refraction index close to -1 is preferred, because it has several advantages such as that for any incidence angle a refracted wave can always be excited, and all rays can be brought to the same focal spot. However, usually size-matched EFC can only be realized through sophisticated methods, such as using more than one kinds of host media [14]. Our aim in this paper is to design a simple PC lens without relying on those sophisticated methods, thus the hole-array structure is our choice. In order to reduce the total reflection power, the EFC size of the PC must be large enough and close to that of the host medium. This consideration leads us to choose $\omega a/2\pi c_t = 0.6$ as the working frequency. If a slightly higher frequency EFC is chosen, the reflection gets higher, and the image intensity gets dimmer. The anisotropic refraction property of the PC looks like a disadvantage, but we will show that a flat lens of this PC can indeed work very well and it can brought the waves emitted by a point source to a image spot of subwavelength wide.

Now we put a point source in front of the lens and study the imaging effect. Simulation results for 9-layer and 13-layer structures are shown in Fig. 3(a)-(c) and (d)-(f), respectively. From (a) to (c) or (d) to (f) the source-lens distance is increased from a to $6a$. According to these simulation results, the shear waves inside the PC indeed propagate along specific directions (the $\pm\pi/6$) as expected. Besides, the thicker the lens, the farther the image locates, consistent with the negative refraction description. Furthermore, when the source moves towards the left, the image also moves towards the left, keeping the source-image distance almost unaltered.

The intensities $|u|^2$ of the displacement field in the focal planes (located at the positions of the image peaks) for the 9-layer and 13-layer lenses are shown in Fig. 4(a) and (b), respectively. In each subplot three source-lens distances ($d = 0.8a$, $3.3a$, and $5.8a$) are examined, and the image widths w defined by their full-width-at-half-maxima (FWHM) are recorded. The results reveal that the lens can really make a subwavelength image of the

point source at the far field zone, although the image width (about 0.6λ) is a little larger than that employing evanescent wave coupling mechanism [22, 35].

The position of focal point can be predicted by considering the refraction of acoustic rays. Although the PC in the chosen frequency cannot be represented by an isotropic effective medium, a formal usage of Snell's law (the consequence of the continuity of the tangential component of wave vector across the host-PC interface) can still help us to find the position of the focal point approximately. The effective refractive index $n = -0.8305$ of the PC at reduced frequency $k_t a / 2\pi = 0.6$ can be derived from the relation $n = -c_t |\mathbf{k}| / \omega = -|\mathbf{k}| / k_t$, here k_t is the radius of the host EFC, and $|\mathbf{k}|$ is the shortest radius (the line segment ΓP in Fig.1(b)) of the PC EFC. We sketch the ray-trace diagram in Fig. 5. The refraction angle are fixed at $\pm\pi/6$, as mentioned above. According to Snell's law, we have $\sin \theta = n \sin(-\pi/6)$, which gives $\theta = 0.4282$ or 24.53° . The distances x_1 and x_2 are related to d_1 and d_2 through the relation $x_1/d_1 = x_2/d_2 = \tan \theta / \tan(\pi/6) = 0.7906$. We thus have a constant source-image distant $d_1 + d_2 + D = 2.265D$, consistent with the results obtained in the wave field simulations. This analysis seems to imply only one incident angle is allowable, which is not the case for waves emitted from a point source. The ray trace calculated in this way represents the route having an extremum phase aggregation, that is, waves interfere constructively along this specific route. If a route slightly deviated from this specific one were used, the phase propagation direction (the direction of \mathbf{k}) and beam propagation direction (the direction of $\langle \mathbf{S} \rangle$) inside the PC would not be parallel to each other. This leads to partially destructive interference and reduce the strength of the ray. A simple glance of Fig. 3 makes these statements more concrete. The predicted positions for the two images (one inside and one outside of the lens) based on the ray formula and those obtained by wave simulations were compared in Fig. 6. A good agreement between these two methods is found, as can be easily checked.

In conclusion, we have proposed a 2D phononic crystal flat lens embedded in solid matrix to achieve far-field subwavelength imaging of off-plane shear waves. The field patterns were computed by using the multiple scattering method, whereas the band structure of the phononic crystal were obtained by using the Dirichlet-to-Neumann map method. Image positions were derived by using ray-trace method, and the results are in good agreement with those from direct wave simulations. Our study has the following novelties. First, our PC lens focuses transverse shear wave, while most of previously proposed PC lenses

focus pressure wave. Second, although we choose aluminum as the host medium, the PC band structure is in fact universal when properly normalized, thus the same kind of lens can be fabricated using other solid matrix materials. Third, we demonstrated that the self-collimation effect of triangular lattice PC can be employed to focus elastic waves, thus circular shaped equal-frequency-contour is not necessary for achieving negative refraction or subwavelength imaging. Our study may provide some insights for designing new kinds of phononic devices.

ACKNOWLEDGEMENT

The author gratefully acknowledge financial support from National Science Council (Grant No. NSC 95-2221-E-008-114-MY3) of the Republic of China, Taiwan.

-
- [1] M. S. Kushwaha, P. Halevi, G. Martinez, L. Dobrzynski, B. Djafari-Rouhani, *Phys. Rev. B* 49, 2313 (1994).
 - [2] M. Kafesaki, M. Sigalas, E. N. Economou, *Solid State Commun.* 96, 285 (1995).
 - [3] M. Torres, F. R. Montero de Espinosa, D. Garcia-Pablos, and N. Garcia, *Phys. Rev. Lett.* 82, 3054 (1999).
 - [4] Zhengyou Liu, Xixiang Zhang, Yiwei Mao, Y. Y. Zhu, Zhiyu Yang, C. T. Chan, Ping Sheng, *Science* 289, 1734 (2000).
 - [5] Yun Lai, Xiangdong Zhang, and Zhao-Qing Zhang, *Appl. Phys. Lett.* 79, 3224 (2001).
 - [6] A. Khelif, B. Djafari-Rouhani, J. O. Vasseur, P. A. Deymier, Ph. Lambin, and L. Dobrzynski, *Phys. Rev. B*, 65, 174308 (2002).
 - [7] Manzhu Ke, Zhengyou Liu, Chunyin Qiu, Wengang Wang, and Jing Shi, Weijia Wen, Ping Sheng, *Phys. Rev. B* 72, 064306 (2005).
 - [8] Shu Zhang, Leilei Yin, Nicholas Fang, *Phys. Rev. Lett.* 102, 194301 (2009).
 - [9] Fu-Li Hsiao, Abdelkrim Khelif, Hanane Moubchir, Abdelkrim Choujaa, Chii-Chang Chen, Vincent Laude, *Phys. Rev. E* 76, 056601 (2007)
 - [10] F. Cervera, L. Sanchis, J.V. Sanchez-Perez, R. Martinez-Sala, C. Rubio, F. Meseguer, C. Lopez, D. Caballero and J. Sanchez-Dehesa, *Phys. Rev. Lett.* 88, 023902 (2001)

- [11] Chao-Hsien Kuo, Zhen Ye, Phys. D: Appl. Phys. 37, 2155 (2004)
- [12] Xiangdong Zhang, Zhengyou Liu, Appl. Phys. Lett. 85, 341 (2004).
- [13] Chunyin Qiu, Xiangdong Zhang, Zhengyou Liu, Phys. Rev. B 71, 054302 (2005).
- [14] A. Sukhovich, Li Jing, J. H. Page, Phys. Rev. B 77, 014301 (2008)
- [15] J. Bucay, E. Roussel, J. O. Vasseur, P. A. Deymier, A-C. Hladky-Hennion, Y. Pennec, K. Muralidharan, B. Djafari-Rouhani, B. Dubus, Phys. Rev. B 79, 214305 (2009)
- [16] A-C. Hladky-Hennion, J. O. Vasseur, B. Dubus, B. Djafari-Rouhani, D. Ekeom, B. Morvan, J. Appl. Phys. 104, 064906 (2008)
- [17] Jing Li, Zhengyou Liu, Chunyin Qiu, Phys. Lett. A 372, 3861 (2008)
- [18] Liang-Shan Chen, Chao-Hsien Kuo, Zhen Ye, Appl. Phys. Lett. 85, 1072 (2004).
- [19] I. Perez-Arjona, V. J. Sanchez-Morcillo, J. Redondo, V. Espinosa, K. Staliunas, Phys. Rev. B 75, 014304 (2007)
- [20] V. Espinosa, V. J. Sanchez-Morcillo, K. Staliunas, I. Perez-Arjona, J. Redondo, Phys. Rev. B 76, 140302 (2007)
- [21] J. Shi, S. S. Lin, T. J. Huang, Appl. Phys. Lett. 92, 111901 (2008)
- [22] Zhaojian He, Feiyan Cai, Yiqun Ding, and Zhengyou Liu, Appl. Phys. Lett. 93, 233503 (2008).
- [23] Xianyu Ao, C. T. Chan, Phys. Rev. E 77, 025601(R) (2008).
- [24] Pi-Gang Luan, Kao-Der Chang, Opt. Exp. 14, 3263 (2006)
- [25] Jianhua Yuan, Ya Yan Lu, J. Opt. Soc. Am. A 23, 3217 (2006).
- [26] Jianhua Yuan, Ya Yan Lu, Opt. Comm. 273 114 (2007).
- [27] C. Goffaux and J. P. Vigneron, Phys. Rev. B 64, 075118 (2001).
- [28] Zhilin Hou, Xiujun Fu, Youyan Liu, Phys. Rev. B 73, 024304 (2006).
- [29] V. Laude, M. Wilm, S. Benchabane, A. Khelif, Phys. Rev. E 71, 036607 (2005).
- [30] J. O. Vasseur, P. A. Deymier, B. Djafari-Rouhani, Y. Pennec, A-C. Hladky-Hennion, Phys. Rev. B 77, 085415 (2008).
- [31] Pi-Gang Luan, Tzong-Jer Yang, arXiv:cond-mat/0409191 (2004).
- [32] K. Sakoda, *Optical Properties of Photonic Crystals*(Springer-Verlag, 2001).
- [33] Shuai Feng, Zhi-Yuan Li, Zhi-Fang Feng, Bing-Ying Cheng, and Dao-Zhong Zhang, Appl. Phys. Lett. 88, 031104 (2006).
- [34] Feng Shuai, Wang Yi-Quan, Li Zhi-Yuan, Cheng Bing-Ying, Zhang Dao-Zhong, Chinese Phy. 1689 (2006).

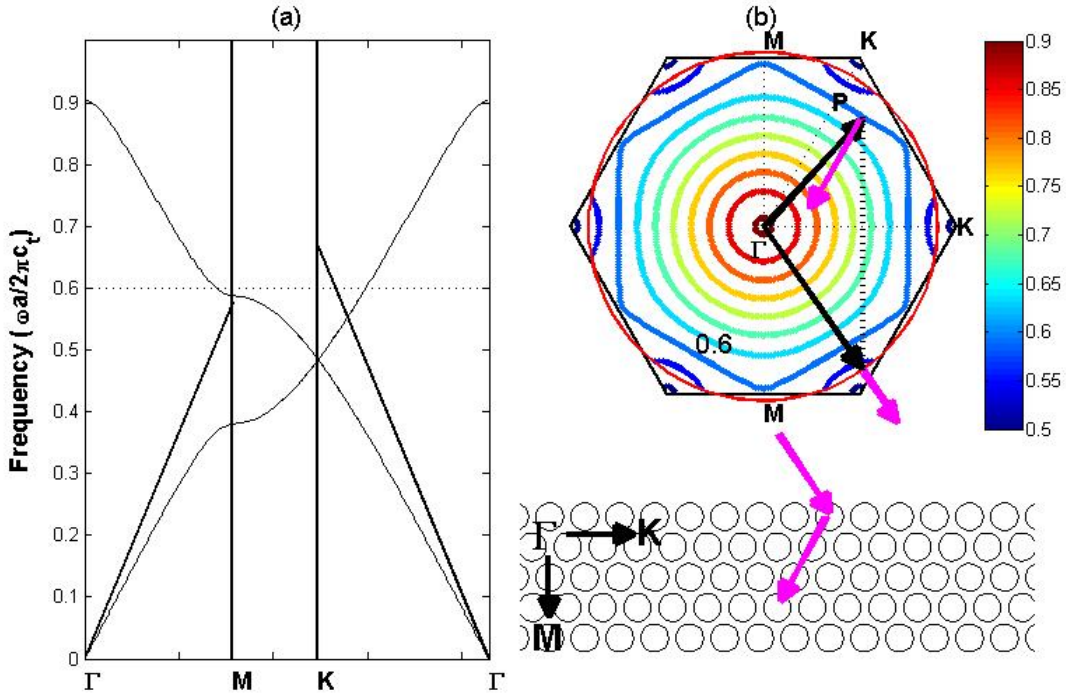


FIG. 1: (a) The band structure of the triangular lattice hole-array PC. (b) The equal frequency contours (EFC) and the refraction diagram. The lattice constant is a , and the radius of the holes is $r_0 = 0.4a$. The two straight lines in (a) are the “sound lines” for the shear wave. The hexagonal blue curve marked 0.6 and the red circle in (b) represent the EFCs of the PC and of the host medium respectively, at reduced (dimensionless) frequency $k_t a / 2\pi = \omega a / 2\pi c_t = 0.6$. The two thick black arrows indicate the \mathbf{k} vectors of the incident and refracted waves. The continuity of the wave phase along the host-PC interface implies that these two \mathbf{k} vectors have the same component along the interface. The two pink arrows represent the energy flow (averaged Poynting vector) directions of the incident and refracted waves. The wave vector length $|\mathbf{k}| = \Gamma P$ is chosen for calculating the effective refraction index n . Note that the direction of the refracted ray (energy flow) is approximately fixed at $\pm\pi/6$. Besides, it is not possible to excite a propagating mode of the PC if the incident angle is larger than $\pi/3$.

[35] Pi-Gang Luan, Kao-Der Chang, *J. Nanophotonics* 1, 013518 (2007).

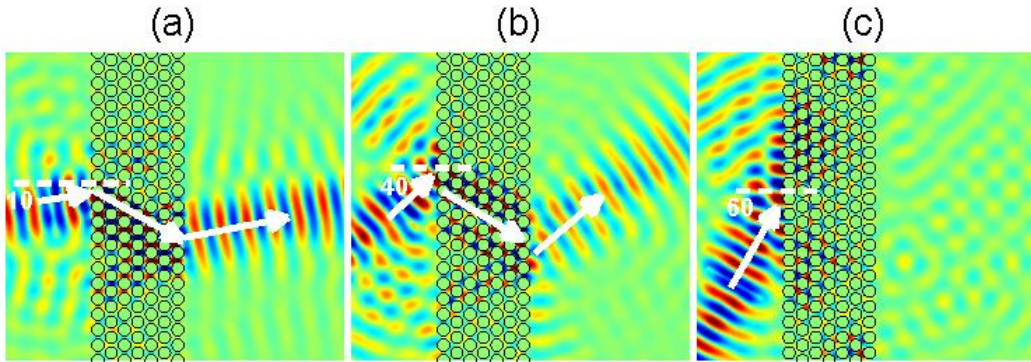


FIG. 2: When a shear wave beam of (dimensionless) frequency 0.6 is incident upon the PC, it gets refracted with angle $\pi/6$ (if the incidence angle is smaller than $\pi/3$) or totally reflected (if the incidence angle is close to or larger than $\pi/3$). The field patterns for incidence angles equal to 10° , 40° and 60° are shown in (a), (b) and (c), respectively.

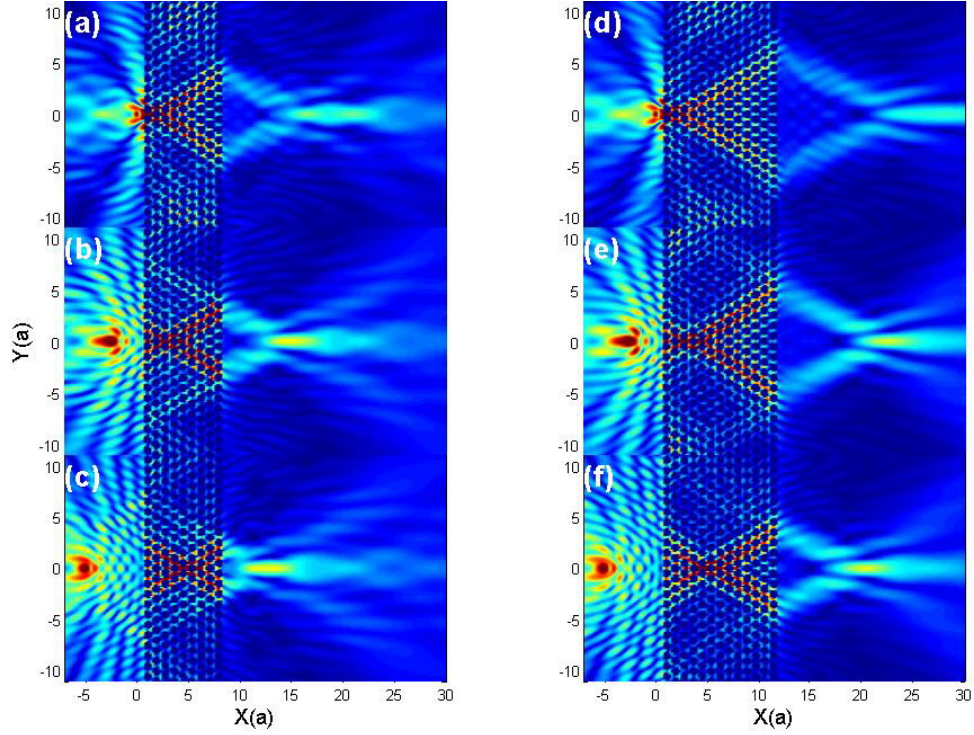


FIG. 3: The displacement field patterns under the illumination of a 2D point source. The center of the first layer of holes is located at $x = a$. The results for the 9-layer structure are shown in (a)-(c). The source is located at $x =$ (a) 0, (b) $-2.5a$, and (c) $-5a$, respectively. Similar simulation results for the 13-layer structure are shown in (d)-(f).

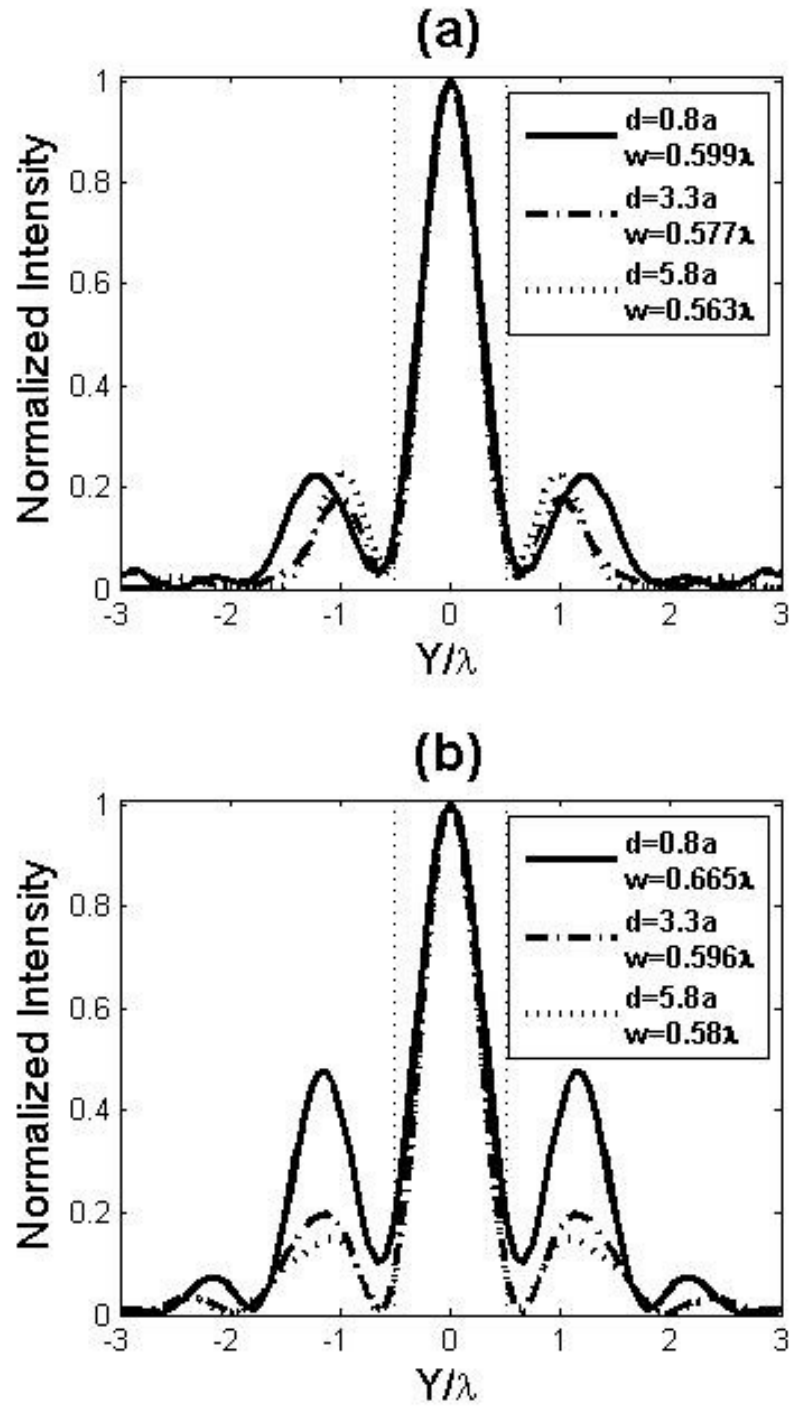


FIG. 4: The shear wave intensities in the focal plane for the (a) 9-layer and (b) 13-layer structures.

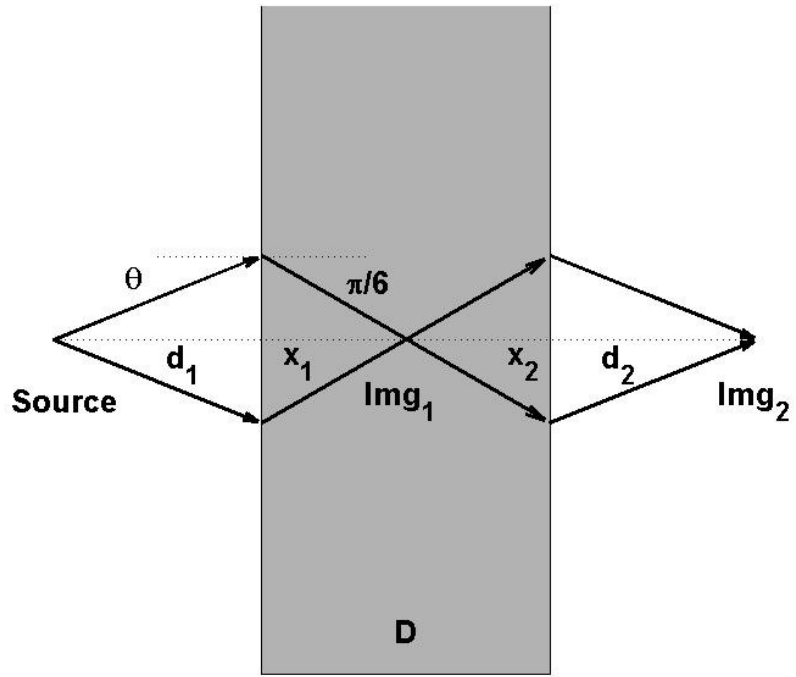


FIG. 5: Refraction of acoustics rays. The refraction angles of $\pm\pi/6$ are expected inside the lens.

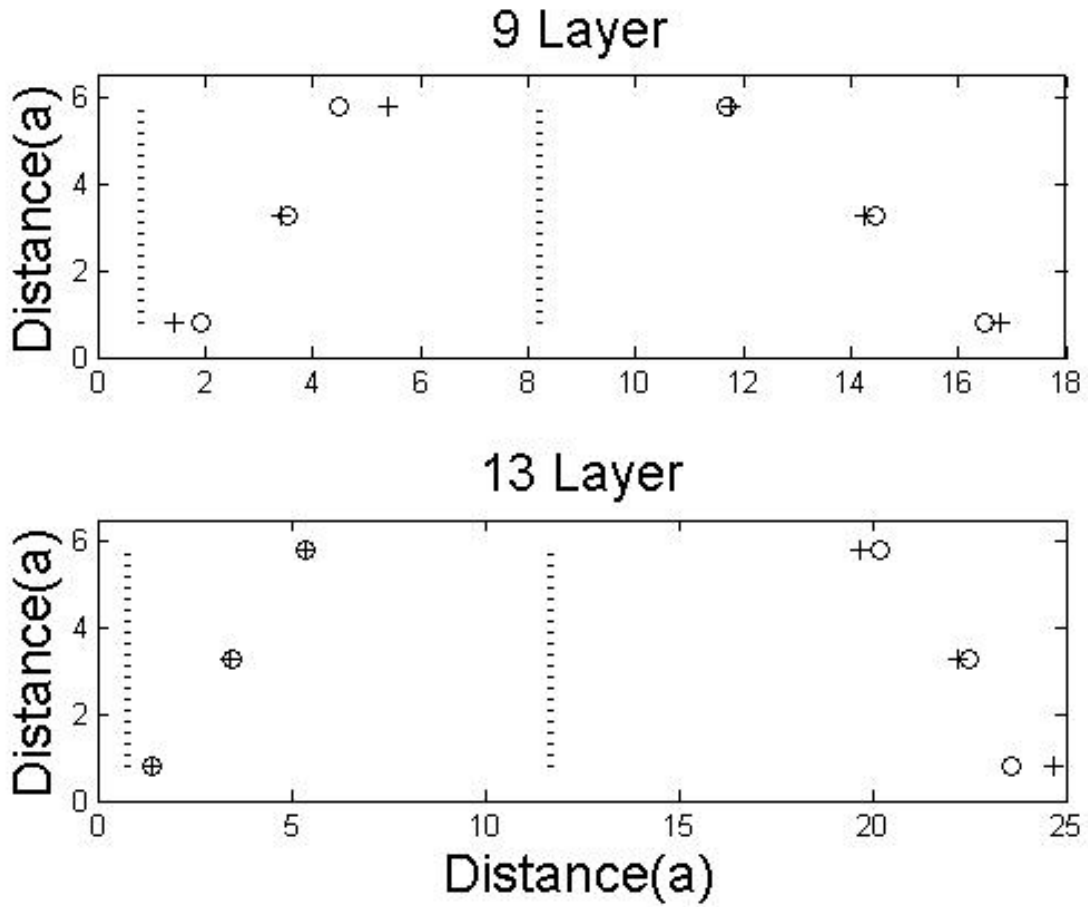


FIG. 6: Comparisons between the predicted (the “+” sign) and the actual (the “o” sign) positions of the images. The vertical axis is the source-lens distance measured from the source location to the center of the first layer of the holes. The horizontal axis is the position of the image. The results for the 9-layer and 13-layer structures are shown in the upper and lower subplots, respectively. The two vertical lines represent the boundaries of the lens.